Expert Systems With Applications 120 (2019) 103–115

Contents lists available at ScienceDirect

Expert Systems With Applications

journal homepage: www.elsevier.com/locate/eswa

Convolutional neural network improvement for breast cancer classification

Fung Fung Ting*, Yen Jun Tan, Kok Swee Sim

Faculty of Engineering and Technology, Multimedia University, Jalan Ayer Keroh Lama, 75450 Melaka, Malaysia

ARTICLE INFO

Article history:
Received 14 March 2018
Revised 11 October 2018
Accepted 5 November 2018
Available online 7 November 2018

Keywords:
Supervised learning
Artificial neural network
Image processing
Medical imaging
Breast cancer classification

ABSTRACT

Traditionally, physicians need to manually delineate the suspected breast cancer area. Numerous studies have mentioned that manual segmentation takes time, and depends on the machine and the operator. The algorithm called Convolutional Neural Network Improvement for Breast Cancer Classification (CNNI-BCC) is presented to assist medical experts in breast cancer diagnosis in timely manner. The CNNI-BCC uses a convolutional neural network that improves the breast cancer lesion classification in order to help experts for breast cancer diagnosis. CNNI-BCC can classify incoming breast cancer medical images into malignant, benign, and healthy patients. The application of present algorithm can assist in classification of mammographic medical images into benign patient, malignant patient and healthy patient without prior information of the presence of a cancerous lesion. The presented method aims to help medical experts for the classification of breast cancer lesion through the implementation of convolutional neural network for the classification of breast cancer. CNNI-BCC can categorize incoming medical images as malignant, benign or normal patient with sensitivity, accuracy, area under the receiver operating characteristic curve (AUC) and specificity of 89.47%, 90.50%, 0.901 ± 0.0314 and 90.71% respectively.

1. Introduction

As United States Breast Cancer Statistics expressed in 2017, an estimated 252,710 new invasive malignancy cases will be analysed in women, alongside 63,410 new patient instances of non-intrusive bosom disease (Breast cancer statistics, 2018). Malaysian woman has one of every 20 opportunities to be diagnosed as breast cancer patient amid her lifetime (Chen & Molloi, 2003). Among all races, Chinese women have the most noteworthy hazard (6.25%) to analyse as breast cancer patient amid her lifetime. The Indian and the Malay women with the lifetime danger of 5.88% and 3.57% then trail this individually.

The rate of survival from breast cancer is highly impacted by malignancy 's phase during diagnosis (Youlden et al., 2012). In this manner, early determination is required to give legitimate treatment to the breast cancer patients and to diminish the dismalness and death rate (Wang, 2017). An elite conclusion for various sorts of tumour is vital for specialists to assist them to choose the appropriate treatment (Chin-Hsing, Ann-Shu, Jiann-Der, & Yang, 1995).

Numerous specialists have applied artificial neural networks for various kinds of disease. Distinctive calculations of artificial neural networks have also been utilized for breast cancer disease identification (Araujo et al., 2017; Mohebian, Marateb, Mansourian, Mañanas, & Mokarian, 2017).

Artificial Neural Network (ANN) instruct the trained system to perform the dedicated task instead of programming the system to perform the defined tasks. The neurons are correlated accordingly to the intricate ANN architecture. The ANN can be configured as unsupervised or supervised.

Mammography is currently the standard and widely used breast cancer medical screening option. However it is not that effective for patient under 40 years old and dense breasts, less susceptible to small tumours (less than 1 mm, approximately 100,000 cells), and gives no indication of breast cancer (Hellquist, Czene, Hjälm, Nyström, & Jonsson, 2015; Onega et al., 2016). The Contrasted-Enhanced (CE) digital mammography provides more diagnostic accuracy than mammography and ultrasound in dense breasts cases, and it is not widely available because it is costly and involves high levels of radiation (Lewis et al., 2017). Ultrasound has been used as an additional medical imaging tool for mammography (Ozmen et al., 2015). Magnetic resonance imaging (MRI) is able to detect small sized lesions that were undetected through mammography. However it is also high priced and has low specificity, hence it may result in the over-diagnosis (Hua, Hsu, Hidayati, Cheng, & Chen, 2015; Roganovic, Djilas, Vujnovic, Pavic, & Stojanov, 2015). The positron emission tomography (PET) is considered the most

* Corresponding author.
E-mail address: sicily.ting@gmail.com (F.F. Ting).

https://doi.org/10.1016/j.eswa.2018.11.008
0957-4174/

accurate technique for visualizing the spread of tumours or their response to therapy (Xavier et al., 2016) .

Three-quarters of National Health Service (NHS) Trusts and Health Boards (76%) says that there is not enough medical specialist to nurse for breast cancer patients (Breast Cancer Care, 2018). Shortage of specialist may lead to late treatment and diagnosis for breast cancer patients. Hence, an informative and early detection for sign of breast cancer can be applied to decrease the recall rate for breast cancer screening tests. President of Malaysian Oncological Society, Dr Matin Mellor Abdullah said that only 110 and 105 of such doctors are serving in both private and public sectors, to take care 31 million of Malaysia citizen, at least 240 cancer specialists in each sector are needed to meet that criteria (MIMS news, 2018).

It was difficult for to use a fixed image processing procedure to detect the various type of mammograms. Various sizes and shapes of fat tissue in the breast result in different contrast from mammogram devices. The primary purpose of this article is to establish new quantitative tools through implementation of machine learning, deep learning techniques that can help decrease the recall rate of screening mammography. The presented Convolutional Neural Network Improvement for Breast Cancer Classification (CNNI-BCC) with a potential impact on changing the balance of routine breast cancer screening procedure towards more benefit and less invasive method. CNNI-BCC is designed to perform effectively in both localize and classification the breast cancer tissue to assist the medical experts in diagnosing the breast cancer.

For the evaluation over the performance of CNNI-BCC, a case study with mammography data sets from breast cancer patients and control subjects is conducted. CNNI-BCC is evaluated according to clinical truths and a comparison with existing techniques. The presented work is organised as follows. The review of the relevant methods is presented in Section 2. In Section 3, the proposed CNNI-BCC method and its variants are explained in detail. In Section 4, the case study is presented, where results from CNNI-BCC and other methods are analysed and discussed. The results of the research are summarized and concluded in Section 5.

2. Related works

Deep learning is part of machine learning (ML) and a special class of artificial neural network (ANN) that resembles the multilayered human cognition system. Deep learning is currently receiving a lot of attention due to its application on health care sector (Lee et al., 2017).

However, given the current availability of big data, improved computing power with graphics processing units (GPUs), and new algorithms to form deep neural network (DNN), many limitations of the ANN have now been resolved. These deep learning approaches have shown impressive performance in imitating humans in various fields, including medical imaging. One of the typical tasks of radiology practice is to detect structural abnormalities and categorize them into disease categories (Qin et al., 2018; Tang et al., 2018; Wang & Summers, 2012).

2.1. Convolutional neural networks (CNN) for breast cancer classification

The Convolutional Neural Network (CNN), which consists of multiple layers of neural computing connections with minimal systematic processing, has yielded significant improvements for computer vision's sector. The CNN global learning process simulates the organization of the animal visual cortex (Hubel & Wiesel, 1968).

CNN's architecture is composed of convolutional, pooling layers and fully connected layers as shown in Fig. 1. The primary purpose of a convolutional layer is to detect edges, lines, and other visual elements like local patterns. The setting of specialized filter operators, called convolutions, are learned through the system. This mathematical operation represents the multiplication of local neighbours from a specified pixel by a certain array of kernel. Through the kernels, this operation imitates the extraction of visual features, such as colours and edges. This is similar to those noted for the visual cortex.

By applying a deep CNN architecture to imitate the natural neuromorphic multilayer network, deep learning can adaptively learn a hierarchical representation of models, from low to high level functions, and then identify the most significant functionalities for a particular model (Krizhevsky, Sutskever, & Hinton, 2012). CNN has the best performance for image classification of a large image repository, such as ImageNet (Krizhevsky et al., 2012).

Because the deep CNN architecture typically involves many layers in the neural network, there may be millions of weight parameters to estimate, thus requiring a large number of data samples for model formation and parameter setting. In general, the minimum requirement for data size depends on the application of radiological images (Krizhevsky et al., 2012).

2.2. Computer-aided detection and diagnosis (CAD)

CAD systems have been widely applied in the context of Picture Archiving and Communication Systems (PACS) (Bogoni et al., 2012; Le, Liu, & Huang, 2009; Welter, Hocken, Deserno, Grouls, & Günther, 2010; Zhou, 2007). This seamless integration of CAD into PACS increases the sensitivity of the reader, without significantly increasing the reading time of the image and thus enhancing the efficiency of the normal practice of radiology.

In summary, current CAD systems have two different parts: detecting and reducing positivity. Typically speaking, detection is mainly based on algorithms specific to the detection task, which results in many potential lesions. This last part is usually based on traditional ML to reduce false positives. Unfortunately, even with these complicated and sophisticated programs, the overall performance of current CAD systems is not efficient enough, which interfere their widespread usage in routine clinical practice. Another important limitation of current CAD systems is sensitivity to imaging protocols and noise (Drew, Cunningham, & Wolfe, 2012; El-Zahraa, El-Gamal, Mohammed, & Ahmed, 2016; Lee et al., 2017). With its known flexibility for image noise and variation in imaging protocols, deep learning has the potential to improve the performance of current CAD at a level useful in everyday practice. Unlike the current CAD system, the deep learning method can provide us with a unique CAD solution. In addition, the unique nature of transfer learning can accelerate the development of the CAD system for various diseases and modalities.

The first reports of deep learning-based CAD systems are suggested by researchers, such as applications on breast cancer (Wang, Khosla, Gargeya, Irshad, & Beck, 2016), lung cancer (Hua, Hsu, Hidayati, Cheng, & Chen, 2015; Kumar, Wong, & Clausi, 2015) and Alzheimer's disease (AD) (Liu et al., 2014; Suk & Shen, 2013; Suk, Lee, & Shen, 2014). They show promising results in terms of detection and staging. In-depth learning has been applied for the identification, detection, diagnosis and risk analysis of breast cancer (Cheng et al., 2016; Kallenberg et al., 2016).

The reviewed studies suggested that medical image annotations is time taken and operator dependent. The screening machine may affect the image quality due to the image noise variance. Manual segmentation is still widely applied as ground truth by medical practitioner. Hence, we present the CNNI-BCC to detect and classify the region of interest of breast cancer lesion. In order to evaluate the performance of the presented works, the comparison between presented works and other reviewed studies (Neuroph, 2018; Saad, Khadour, & Kanafani, 2016; Tan, Sim, & Ting, 2017) are conducted

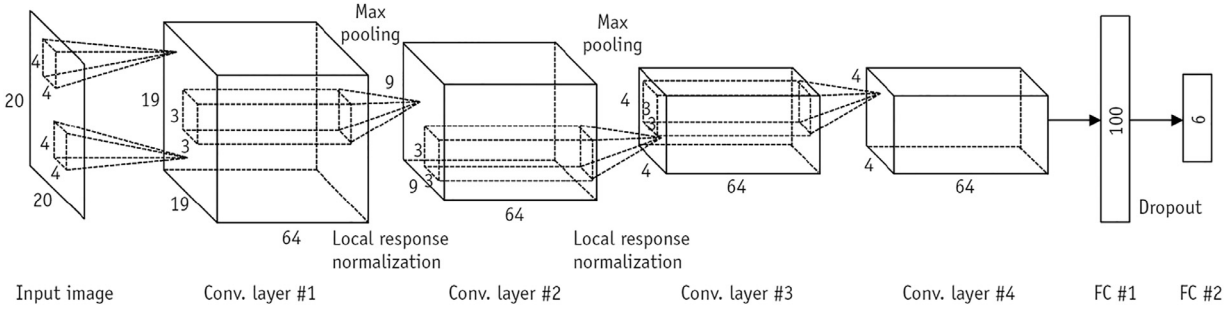

Fig. 1. Architecture of convolutional neural networks, including input, Conv., and FC layers. Conv. = convolutional, FC = fully connected.

and tabulated at Section 4.0. The previous work is experimental work, which validates the MIAS results with designed CNN architecture. The current work presents novel Interactive detection-based lesion locator (IDBLL) to preform two-phase classification on breast cancer lesion to enhance the accuracy of classification.

2.3. Contribution

Several addressed challenges in reviewed studies are:

(1) The tedious annotation produces an additional source for errors in data labels
(2) Lesion margins are ambiguous, creating controversial annotations
(3) CAD system often affected by sensitivity to imaging protocols and noise
(4) Medical data annotations is time consuming

The following major contributions are addressed: (1) We present a deep CNN for classification of a mammograms according to the patch features; (2) The presented works further suggests detection of the lesions through designed Interactive detection based lesion locator (IDBLL); (3) CNNI-BCC provides assistance to medical experts in breast cancer diagnosis.

Our method suggests the following advantages: (1) Decomposing the images into patches; (2) The patch-based approach allows processing of non-rectangular regions in the image by masking of certain areas, with simply excluding patches from the collection; (3) A combined pre-trained CNN allows training on small data sets; (4) The presented CNNI-BCC utilise the patch feature relevance to detect and classify the lesion region and category.

In this paper, an automated method of classifying breast cancer is presented, it is called Convolutional Neural Network Improvement for Breast Cancer Classification (CNNI-BCC). It is designed to aid medical experts in the breast cancer classification.

3. Materials and methods

3.1. Materials

The applied digital mammogram databases was prepared and provided by Mammographic Image Analysis Society (MIAS) (Mammographic Image Analysis Society, 2018). The mammogram was provided in Portable Gray Map (PGM) image format. The medical doctor verified and diagnosed ground truth data that was provided. For this study, 21 benign cases, 17 malignant cases and 183 normal cases are involved. The raw digital mammogram image accompanied with labelled ground truth data is shown on Fig. 2. Comparative experiments were conducted between the presented work and the commercial software named Neuroph (The Neuroph, 2018) which was used as a semi-automatic segmentation algorithm.

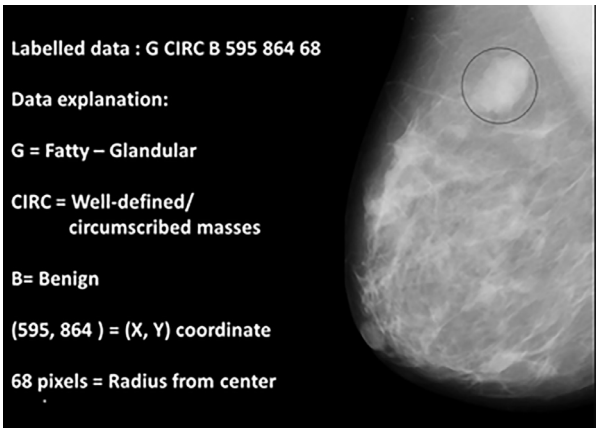

Fig. 2. Mammogram image with labelled data.

The provided ground truth information includes the background tissue, type of abnormality present, the abnormality's severity, *x*-axis, *y*-axis coordinates of the abnormality centre, and the abnormality's radius measured in pixels.

3.2. Methods

When training and testing on a shuffled dataset with an even distribution of normal, benign, and malignant data points, we observe the best recall and precision on a CNN. This convolutional neural network consists of 1 input layer, 28 hidden layers and 1 output layer. The input layer is used original size abnormally cancer images in RGB channels. A convolutional layer is located at first hidden layer for feature map extraction. A dropout rate of 0.5, a learning rate of 0.002, fully connected hidden layer of 1024 neurons, and Rectified Linear Units (ReLUs). Data augmentation is performed on the image patches to overcome the overfitting issue faced by other researchers. ReLUs is applied as nonlinear layers in the fully connected layer section. The process is initialized with annotations and over patches. The stopping criterion was set to 25–35 epochs according to a validation set. The architecture of CNNI-BCC is shown in Fig. 3.

Total 30 layers CNN operations is involved the description and input size for each layer is tabulated in Table 1.

Fig. 4 shows the overall procedure of the CNNI-BCC method. It consists of three main steps: (a) feature wise pre-processing (FWP), (b) convolutional neural network (CNN) -based classification (CNNBS), (c) interactive detection based lesion locator (IDBLL).

3.2.1. Feature wise data augmentation (FWDA)

The raw digital mammogram image size is 1024×1024 pixels. In order to process the whole image, tremendous amount of computation works and time are required. Hence, feature wise pre-

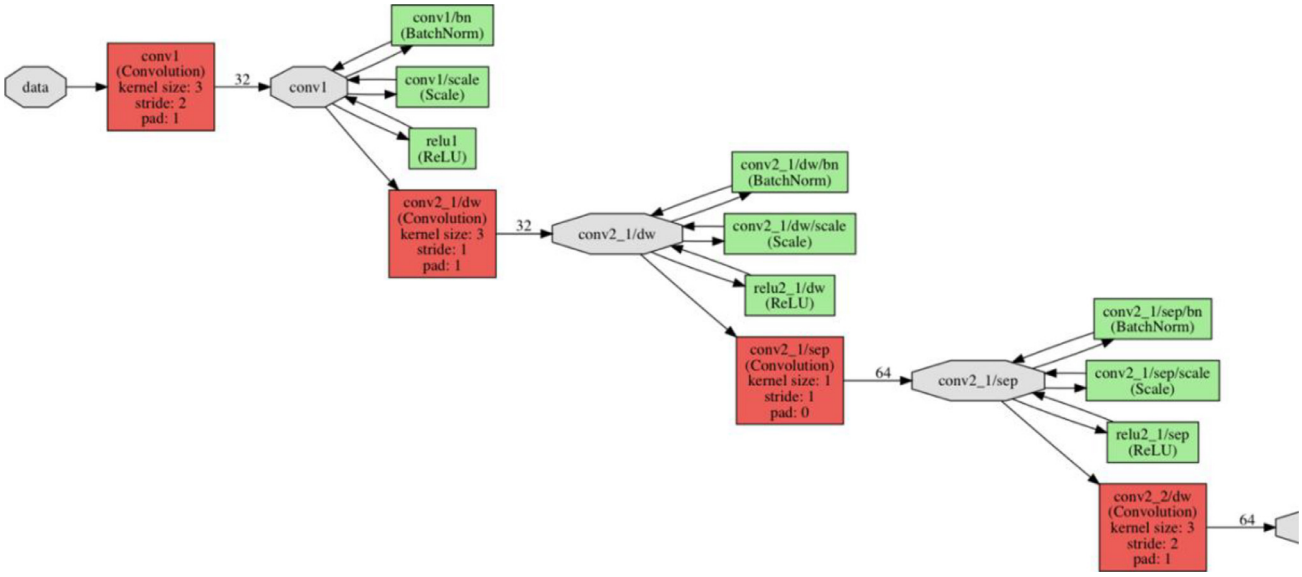

Fig. 3. shows the neural network architecture section of the CNNI-BCC.

Table 1
The layers 'description for CNNI-BCC architecture.

Layer's number	Type/Stride	Filter	Input size
1	Conv /s2	$3 \times 3 \times 3 \times 32$	$224 \times 224 \times 3$
2	Conv dw /s1	$3 \times 3 \times 32$ dw	$112 \times 112 \times 32$
3	Conv/ s1	$1 \times 1 \times 32 \times 64$	$112 \times 112 \times 32$
4	Conv dw /s2	$3 \times 3 \times 64$ dw	$112 \times 112 \times 64$
5	Conv /s1	$1 \times 1 \times 64 \times 128$	$56 \times 56 \times 64$
6	Conv dw /s1	$3 \times 3 \times 128$ dw	$56 \times 56 \times 128$
7	Conv /s1	$1 \times 1 \times 128 \times 128$	$56 \times 56 \times 128$
8	Conv dw /s2	$3 \times 3 \times 128$ dw	$56 \times 56 \times 128$
9	Conv /s1	$1 \times 1 \times 128 \times 256$	$56 \times 56 \times 128$
10	Conv dw /s1	$3 \times 3 \times 256$ dw	$28 \times 28 \times 256$
11	Conv /s1	$1 \times 1 \times 256 \times 256$	$28 \times 28 \times 256$
12	Conv dw /s2	$3 \times 3 \times 256$ dw	$28 \times 28 \times 256$
13	Conv /s1	$1 \times 1 \times 256 \times 512$	$14 \times 14 \times 256$
14–22	Conv dw/ s1Conv /s1	3x3x512 dw1x1x512x512	14x14x512
23	Conv dw /s2	3x3x512 dw	14x14x512
24	Conv /s1	1x1x512x1024	7x7x512
25	Conv dw /s2	3x3x1024 dw	7x7x1024
26	Conv /s1	1x1x1024x1024	7x7x1024
27	Average Pool /s1	Pool 7x7x	7x7x1024
28	Fully Connected/s1	1024x1000	1x1x1024
29	Softmax/s1	Classifier	1x1x1000

processing (FWP) is designed to shorten the CNN process time by pre-processing the input images beforehand. FWP is applied to divide the input images into smaller image patches. The images patches are rotated clockwise to 90°, 180°, 270° and 360°. Every rotated patch is flipped vertically. Henceforth, an input mammogram image will generate eight image patches. The MIAS provides the diagnosis result and ground truths.

3.2.1.1. Subsampling. The abnormality or the region of interest (ROI) of mammogram is extracted and labelled as image patches as shown in Fig. 5. The abnormality information given by MIAS is utilised to specify the ROI centre. Once the ROI is extracted, the image feature patch will be processed into 8 different patches according to the rotation angle and the flipped position. The annotation of the abnormality is exported as XML files along with information like *x*-axis, *y*-axis coordinates of the abnormality centre and breast cancer abnormality classes.

The training data is prepared through patches generated from delineated abnormal tissue's region of interest (ROI). Total 8 feature patches will be generated from one mammogram image. The image patches from benign cases, malignant cases and normal cases are shown on Figs. 6–8.

The resolution of training data patch is 128×128 pixels. Image transformation is applied to subsampling the 1024×1024 pixels input mammogram images. The convoluted image patches provide features in various direction to enhance the classification accuracy for the training data.

The ROI is extracted from the background to implement the classification process. The black background of the mammogram image may affect the condition of the training data and leads to inefficient feature learning for the CNN. Some samples of affected training data patches are shown at Fig. 9.

The detailed algorithm of feature wise data augmentation (FWDA) is shown in Table 2.

The FWDA is utilise to generate larger dataset patches capacity to decrease the likelihood of overfitting occurrence. Augmented image patches can improve the classification performance by proving more feature information in various image coordination.

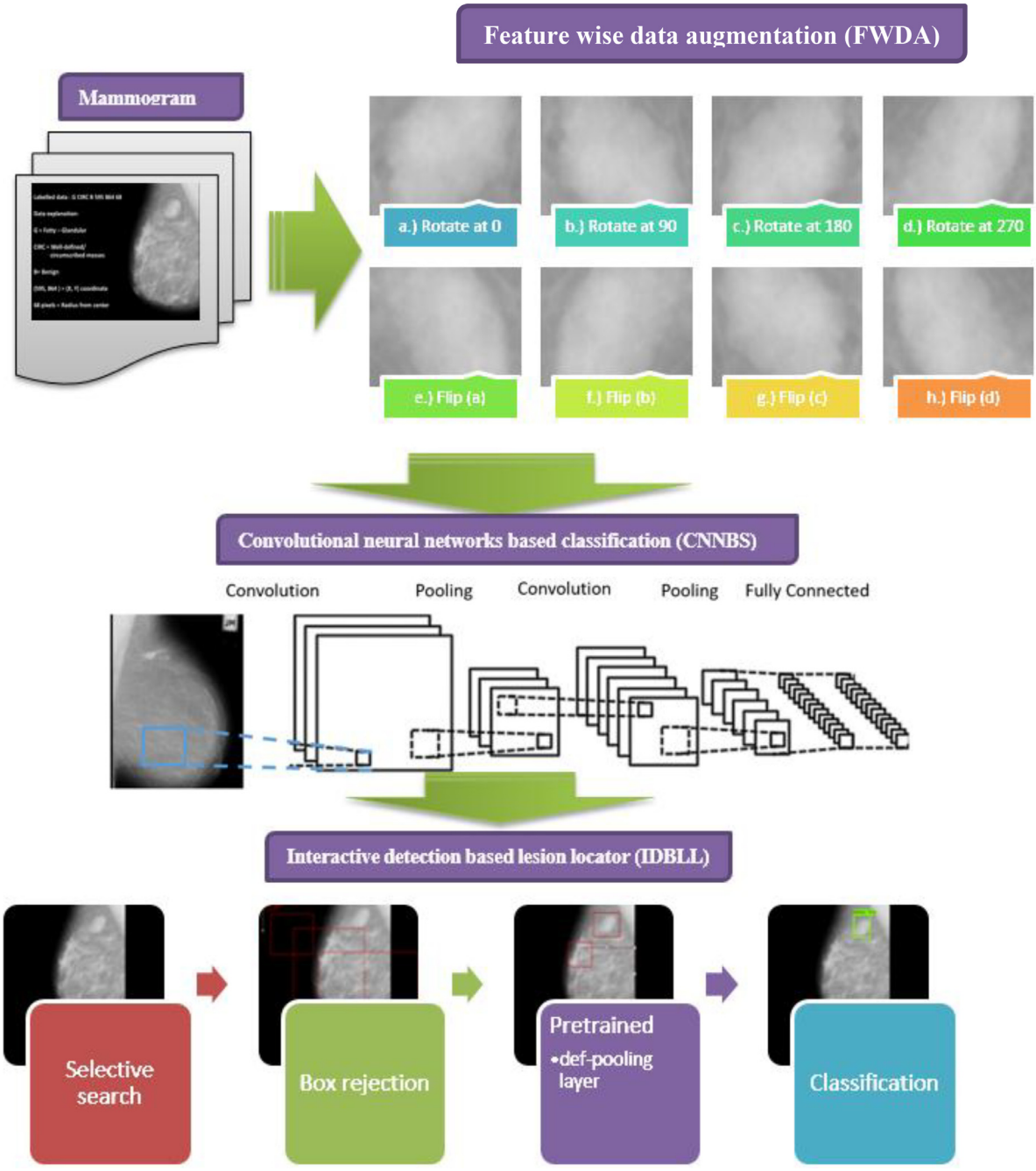

Fig. 4. The overall architecture of the presented work.

Table 2

Algorithm 1: Feature wise data augmentation (FWDA)	
1:	Read Input Mammogram for benign M_b, malignant, M_m and normal patients M_n.
2:	Pre-process the input images, M_b, M_m, M_n.
3:	M_b, M_m, M_n subsample according to transformation
4:	For M_b, ROTATE to 90°, 180°, and 270° For M_m, ROTATE to 90°, 180°, and 270° For M_n, ROTATE to 90°, 180°,and 270°
5:	Till all images had been re-aligned
6:	Perform FLIP on all aligned images.
7:	Write all images in as subsampled images
8:	Repeat on other training data.
9:	End

Table 3

Algorithm 2: Convolutional neural networks based classification (CNNBS)	
1:	Set parameters: $Error_{Max}$,$Iteration_{max}$,$Rate_{learning}$
2:	Set $CNNLayer_{input}$, $CNNLayer_{conv}$, $CNNLayer_{pooling}$, $CNNLayer_{dense}$and $CNNLayer_{output}$
3:	Read $Data_{Training}$, send input data to the CNNBS network.
	// CNNBS data training phase
4:	For every input data,
5:	Compute differences through between predicted output value and the estimated output value for the input
6:	Change *weights* value accordingly for all neurons by applying the obtained *error*
7:	Repeat loop until acquired certain threshold
8:	End For loop
9:	End

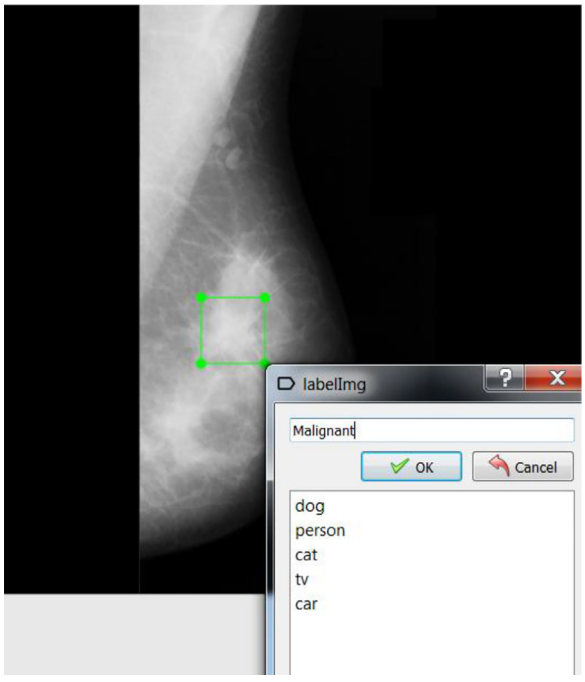

Fig. 5. Labelling process on raw input mammogram image.

3.2.2. Convolutional neural networks based classification (CNNBS)

CNN is composed of neurons that are arranged according weight and biases. Every neuron receives inputs data. The dot product is performed and trailed by non-linearity. The entire network always defines a single differentiable score function. The CNN layers architecture neurons are arranged in three different dimensions: height, width, and depth as shown in Fig. 10.

CNNI-BCC architecture is constructed from one input layer, two hidden layer, and one output layer. The training dataset patches from FWDA served as input data for the designated input layer. In the presented works, the input training data is measured in 48 pixels x 48 pixels x 1 in dimension. The hidden layer of presented CNNI-BCC has convolutional layer, rectified linear unit (ReLU) layer, pooling layer, and dense (fully connected) layer.

In the convolutional layers, the designated convolution filters is applied on input image. The filtering process is performed on region-by-region basis. For every sub region, the convolution matrix operations is employed to generate the value in order to form output feature map. This layer is commonly referred as sets of weights as a filter or a kernel that is convolved with the input. Rectified linear unit (ReLU) activation function is applied on convolution layer to introduce nonlinearities into the model through generated output map as shown in Fig. 11.

The pooling layer has played a crucial role for CNNI-BCC. Several nonlinear functions are employed to enhance pooling among which max pooling is the commonly used functions. It divides the input image patch into a set of non-overlapping rectangles. Then, for every sub-region, the display is set at maximum. The exact feature location is less important than its approximate location relative to other features. The number of parameters and the amount of computation in the network can be reduced through pooling layer, and thus control the over-learning. The grouping operation provides another type of translation invariance.

Back propagation is utilised in CNNI-BCC for the neuron weight, which is updated on last closest value. The computed error is applied in the model for enhance accuracy.

Rectified linear units (ReLUs) had been applied for the hidden layers. If the input is less than zero, the rectified linear unit has output 0. The output equals to input if the input is greater than zero. ReLU activation function is shown at Eq. (1),

$$f(x) = \max(x, 0), \tag{1}$$

The employed softmax function compresses the outputs of each neuron to be in between 0 and 1. It is also acted similar to the sigmoid function. However, it also divides each output such that the total sum of the outputs is equal to 1.The generated output is a categorical probability distribution. It computes the probability so that any of the classes is true.

$$\sigma(z)_j = \frac{e^{Z_j}}{\sum_{k=1}^{K} e^{z_{k'}}} \tag{2}$$

where z defines a vector of the inputs to the output layer .If there are 10 output units, then there are 10 elements in z. The j indexes the output units, so that $j = 1, 2, \ldots, K$.

Final layer in CNNBS is fully connected layer. It is usually called as a decision layer. For CNNBS, the dense layer is connected last

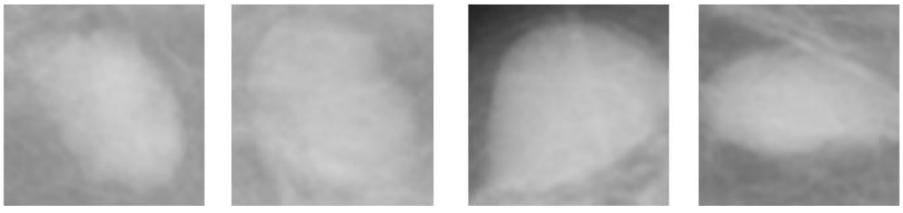

Fig. 6. Training data patches for benign cases.

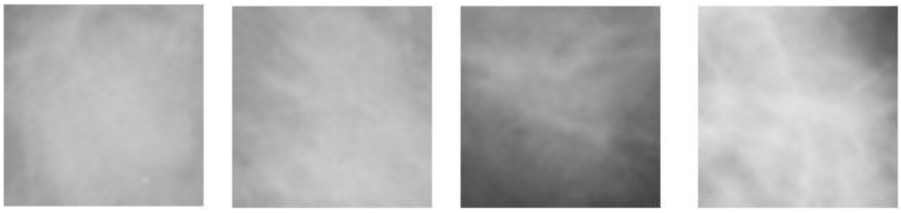

Fig. 7. Training data patches for malignant cases.

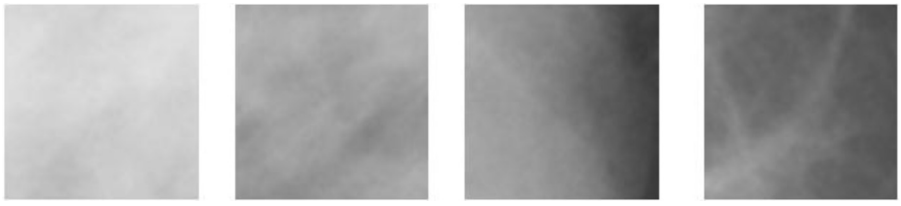

Fig. 8. Training data patches for normal cases from healthy patient.

Fig. 9. The affected training data.

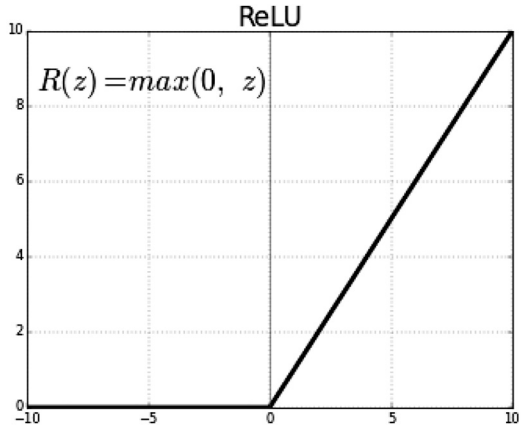

Fig. 11. Rectified linear unit (ReLU) activation function applied in Convolutional Neural Network Improvement for Breast Cancer Classification (CNNI-BCC).

hidden layer. Three possible output categories are 0 for the normal, 1 for the benign, and 2 for the malignant. Fig. 12 shows the architecture of proposed approach CNNBS. The MIAS dataset is divided into training set and testing set. FWDA is applied to increase the data pool to reduce the overfitting occurrence. The trained model is utilise during testing phase for classification status. The trained model is further implemented through Interactive detection based lesion locator (IDBLL) in Section 3.2.3.

Depth wise separable convolutional layer (DSC) has two batches. One batch is for the normalization, and the other is for rectified linear unit (ReLU) which is followed with all layers of the CNNBS. The flow of depth wise separable convolution (DSC) layer is shown at Fig. 13.

Depth wise convolution and Pointwise Convolution are involved for Depth wise separable convolution. A 3×3 convolution filter is applied as factorized convolution per input image. It will only use to filter a single depth of the input map. Depth wise separable convolution will collect the feature layer by layer. The Depth wise convolution is as shown at Fig. 14.

Depth wise separable convolution will perform the convolution separately to be 3-layer smaller output for RGB image as shown in Fig. 15. However, in order to reduce the X and Y pixel, the number of layers remained the same.

Pointwise convolution is a filter that applied for data combination as shown in Fig. 16. The feature of the map is increased with same X and Y pixel as shown in Fig. 17. The primary purpose of Pointwise convolution is to generate more features for better classification on the detected object. The plotted receiver operating characteristic (ROC) curve for CNNI-BCC is shown in Fig. 18.

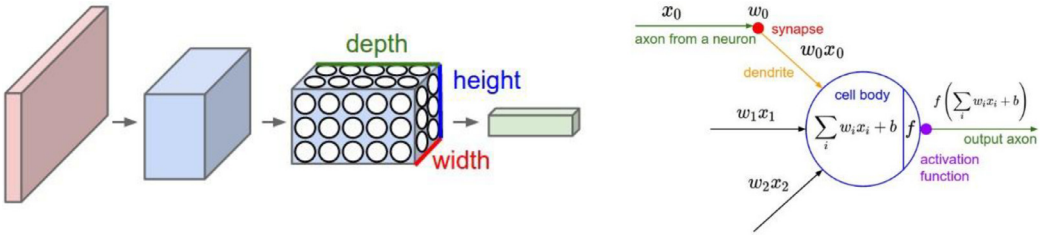

Fig. 10. The neuron arrangement of Convolutional Neural Networks. (Karpathy, 2018).

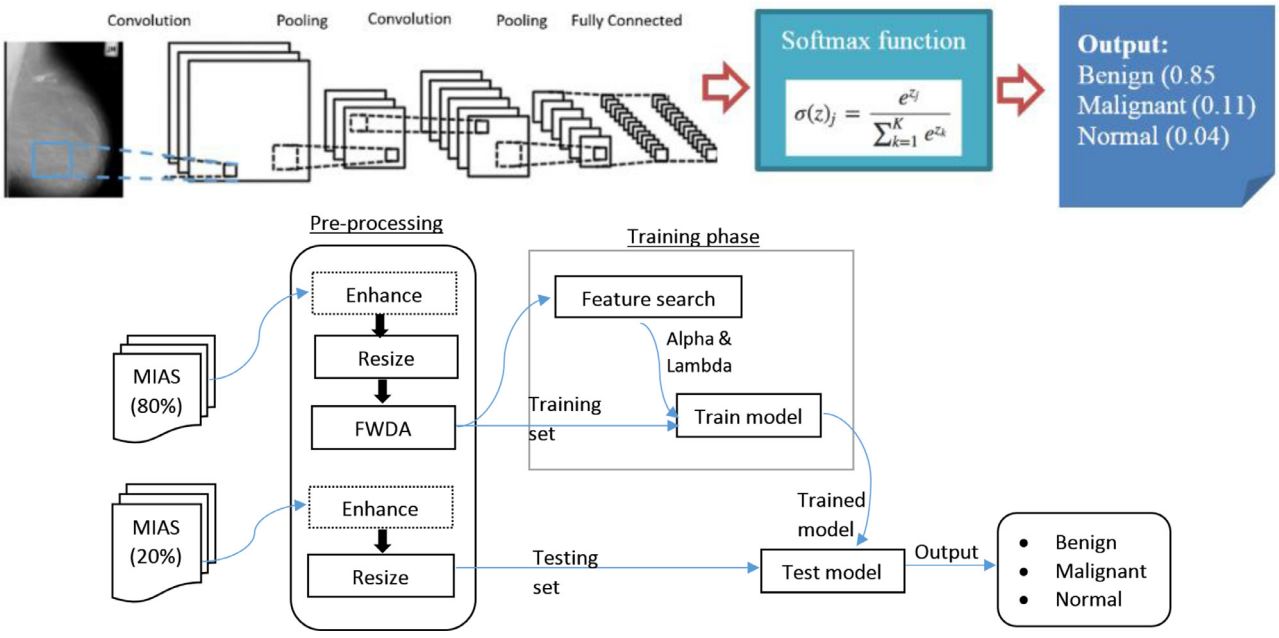

Fig. 12. The flow of CNNBS.

Fig. 13. The flow of depth wise separable convolution (DSC) layer (Goodfellow, Bengio, & Courville, 2016).

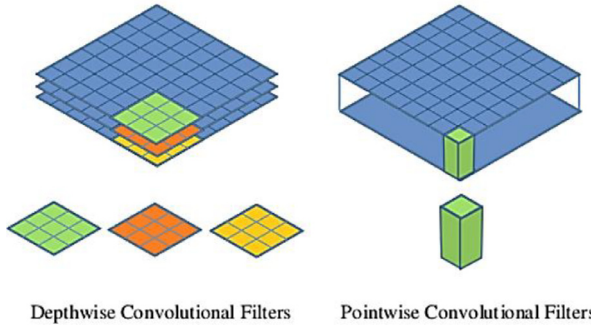

Fig. 14. The illustration of Depth wise convolution and Pointwise Convolution (Goodfellow et al., 2016).

3.2.3. Interactive detection based lesion locator (IDBLL)

Interactive detection based lesion locator (IDBLL) utilises Single Shot MultiBox Detector (SSD) for object detection in images to use single deep neural network. IDBLL can detect object by using predicted bounding boxes. The features are resampled for each predicted bounding box, and classify them through IDBLL.

The primary advantage of IDBLL is the prediction is based on every convolution for each feature map for better estimation. The total amount of estimated anchor point is decreased in a smaller pixels feature map. During the training phase of IDBLL, original 1024×1024 pixels image and annotation that are used. Default boundary boxes are matched with the annotation to give a positive value in the area. Hence, the background and non-relevant regions are given negative intensity value. IDBLL uses this information to

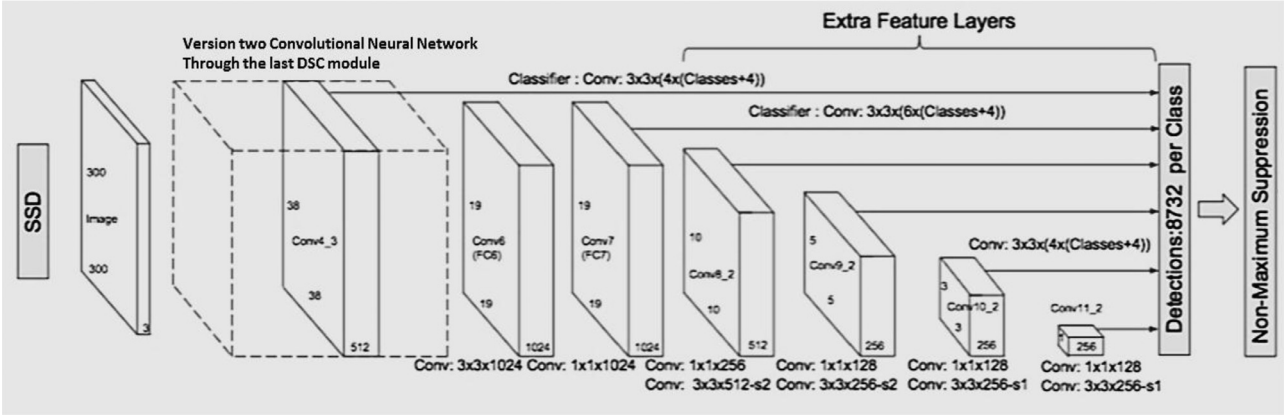

Fig. 15. The illustration of Interactive detection based lesion locator (IDBLL) (Liu et al., 2016).

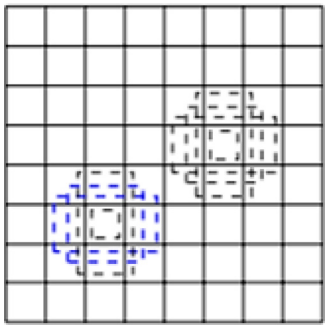

Fig. 16. 8×8 feature map (Liu et al., 2016).

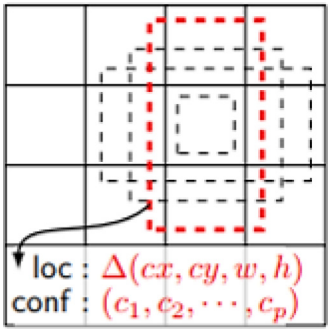

Fig. 17. 4×4 feature map (Liu et al., 2016).

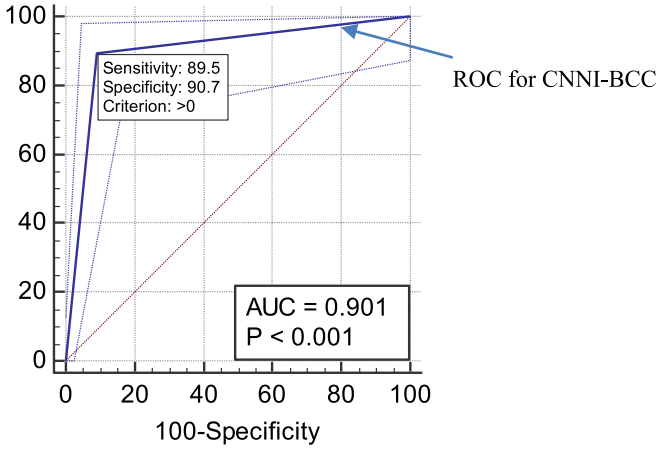

Fig. 18. The plotted receiver operating characteristic (ROC) curve for CNNI-BCC.

differentiate the dissimilarities between breast cancer region and background.

The total amount of estimated anchor point is decreased in a smaller pixels feature map. During the training phase of IDBLL, original 1024×1024 pixels image and annotation that are used. Default boundary boxes are matched with the annotation to give a positive value in the area. Hence, the background and non-relevant regions are given negative intensity value. IDBLL used these information to differentiate the dissimilarities between breast cancer region and background.

IDBLL applies pre-defined set of bounding boxes at each location of image with different size's ratio. Hence, during the training phase, it will match the default boxes with the given label and learn the differences of the object with features surrounded it. IDBLL will compare the detected boxes with trained boxes to extract the feature map of CNNBS.

The algorithm of IDBLL is shown as Table 4.

Table 4

Algorithm 3: Interactive detection based lesion locator (IDBLL)	
1:	Set size for $IDBLL_{BoundingBox}$
2.:	Read $Data_{Testing}$
3:	For every point p of $Data_{Test}$ ($R[i,j]x\ C[i,j]x$ *No.of Pixel*),
4:	Apply $IDBLL_{BoundingBox}$
5:	Check if the $Pixel_{Surround}$ match the features
6:	Compare the pixel feature with Trained CNNBS
7:	Else
8:	Include p in LIST[p]
9:	End For loop
10:	$IDBLL_{BoundingBox}$ (LIST[v])
11:	Repeat for other test mammogram images
14:	End

4.0. Experimental study and results discussion

The experiments are conducted on 221 real patient mammogram. Mammographic Image Analysis Society (MIAS, 2018) provides the data. The presented method performance is assessed in terms of the area under the receiver operating characteristic (ROC) curve, sensitivity, accuracy and specificity.

$$Sensitivity = TP/(TP + FP), \tag{3}$$

$$Specificity = TN/(FP + TN) \tag{4}$$

$$Accuracy = (TP + TN)/N \tag{5}$$

where, N represents the total number of patients, TP defined true positive value, TN denoted true negative value, FN is the false negative while FP represented false positive value.

With CNNI-BCC, 34 out of 39 positive cases have been identified as true positive cases, while 166 over 183 negative cases have been identified as true negative cases. The sensitivity, specificity, and accuracy scores are 89.47%, 90.71%, and 90.50% respectively. The experiments are conducted to analyse the performance between presented work and existing reviewed methods. The results are tabulated as Table 5.

The adaboost (Saad et al., 2016) is tested on MIAS dataset and achieve 78.12%, 87.5% and 81.25% in sensitivity, specificity and accuracy. BPNN (Saad et al., 2016) accuracy is lower than adaboost. Both methods utilise the supervised neural network setup for training and testing phases. However, they results may be affected by how they pre-process the MIAS dataset images. Various pre-process methods yield different effect for the classification task.

Based on 221 number of patients, the sensitivity, specificity, accuracy for Neuroph (The Neuroph, 2018) are 97.37%, 22.95% and 35.75% respectively. The false positive rate for Neuroph (The Neuroph, 2018) is 77.05%. The high false positive rate may due to the difficulty faced for the normal mammogram. The dense mass of the breast region of younger patient may be miss-classified at breast cancer lesion. The comparison of the ROC curves between CNNI-BC and Neuroph (The Neuroph, 2018) are discussed at Section 4.3.

The BCDCNN (Tan et al., 2017) is the previous presented method. BCDCNN achieved low in sensitivity, specificity and accuracy in comparison to the current proposed approach. The FWDA and IDBLL help to improve the performance of the proposed approach, CNNI-BCC. By having a two phase classifications on CNNBS and IDBLL, the classification accuracy can be improved. The receiver operating characteristic (ROC) curve statistics show promising performance of the proposed approach.

According to Table 6, the area under the ROC curve for CNNI-BCC is 0.901 ± 0.0314. The significance level P is equal to 0.5

Table 5
The comparison between Convolutional Neural Network Improvement for Breast Cancer Classification (CNNI-BCC) and reviewed studies.

Methods	Sensitivity (%)	Specificity (%)	Accuracy (%)	False positive rate	False negative rate
Adaboost	78.12	87.5	81.25	–	–
BPNN	75.00	81.25	77.08	–	–
Neuroph MLP	97.37	22.95	35.75	77.05	2.63
BCDCNN(Version 1)	35.32	35.43	38.45	64.57	64.68
BCDCNN(Version 2)	54.32	54.36	54.35	45.64	45.68
BCDCNN(Version 3)	82.68	82.73	82.71	17.27	17.32
CNNI-BCC	**89.47**	**90.71**	**90.50**	**9.29**	**10.51**

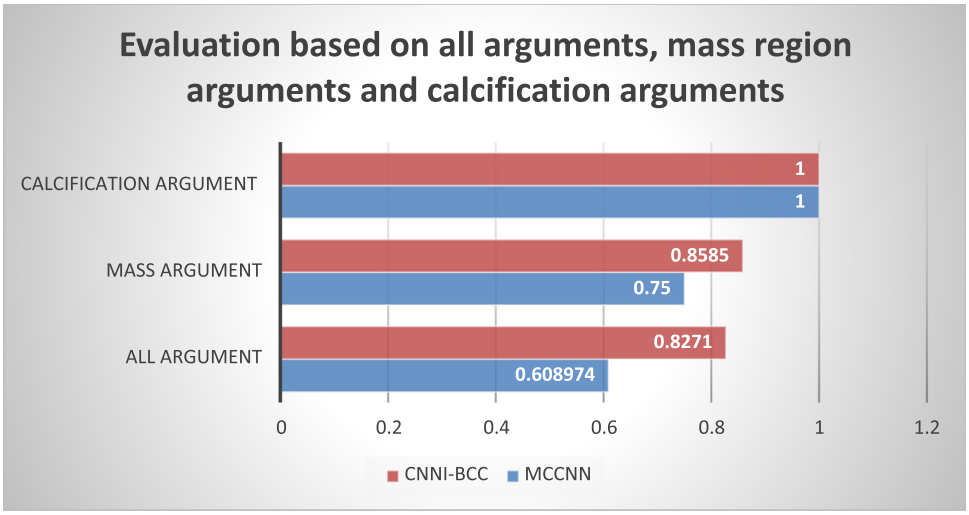

Fig. 19. Comparison between CNNI-BCC and MCCNN (Henry, 2018) on all arguments, mass region arguments and calcification arguments images.

Table 6
The ROC curves statistics for Convolutional Neural Network Improvement for Breast Cancer Classification (CNNI-BCC) against ground truths.

Statistics	Value
Area under the ROC curve (AUC)	0.901
Standard Error [a]	0.0314
95% Confidence interval [b]	0.854 to 0.937
z statistic	12.779
Significance level P (Area = 0.5)	<0.0001
Youden index J	0.8018
Associated criterion	>0
Sensitivity	89.47
Specificity	90.71

is < 0.0001, hence indicates that presented work has high performance. The area under the ROC curve (AUC) calculation summarized the ROC curve analysis into a scalar value, which is a value ranged between 0 and 1. The nearer the AUC score to value 1, the better the overall performance of the application. AUC is calculated as shown in Eq. (6):

$$AUC = \int_{\infty}^{-\infty} TPR(T)\left(-FPR'(T)\right)dT = \int_{-\infty}^{\infty}\int_{-\infty}^{\infty} I\left(T' > T\right) f_1\left(T'\right) f_0(T)\,dT'\,dT = P(X_1 > X_0), \quad (6)$$

where the threshold in which the instance is classified as "positive" if $X > T$, and "negative" otherwise; X_1 is the score for a positive instance, and X_0 is the score for a negative instance.

The disease prevalence is 17.2% which represents the relevance between positive group and negative group. In this case, the positive group is the diagnose breast cancer patients while the negative group denotes the healthy or normal patients.

The Youden index confidence interval is calculated as predictive behaviour according to the collected data. The index is defined as:

$$J = \max\{sensitivity_c + specificity_c - 1\}, \quad (7)$$

where c ranges over all possible criterion values. While J defines maximum vertical distance between the ROC curve and the diagonal line.

The criterion value corresponding with the Youden index (J) shown in Table 7 is the optimal criterion value only when disease prevalence is 50%. So, equal weight is given to sensitivity and specificity, and costs of various decisions are ignored. The bootstrapped 95% confidence interval is calculated for the Youden index and its associated criterion value.

4.1. Evaluation based on all arguments, mass region arguments and calcification arguments

The input patch for CNNI-BCC is 128×128 pixel. CNNI-BCC is constructed from convolution layer with kernel size 5×5 filter, pooling layer with pool size 2×2 filter and strides of two, learning rate with 0.003, training step with 20,000.

For this evaluation, the testing data is categorised into three different categories, namely all arguments, mass region arguments and calcification arguments. For all arguments, all testing mammogram images are involved. For the mass only argument, only the breast region mass section mammograms are involved. The mammograms with the calcification will be involved under calcification argument category. These three categories of testing data are fed as input to the CNNI-BCC and the Mammogram Classification Using Convolutional Neural Networks (MCCNN) (Henry, 2018). By referring to Fig. 19, CNNI-BCC excels than the MCCNN for mass argument images and all arguments images at 0.8585 and 0.8271 accuracy.

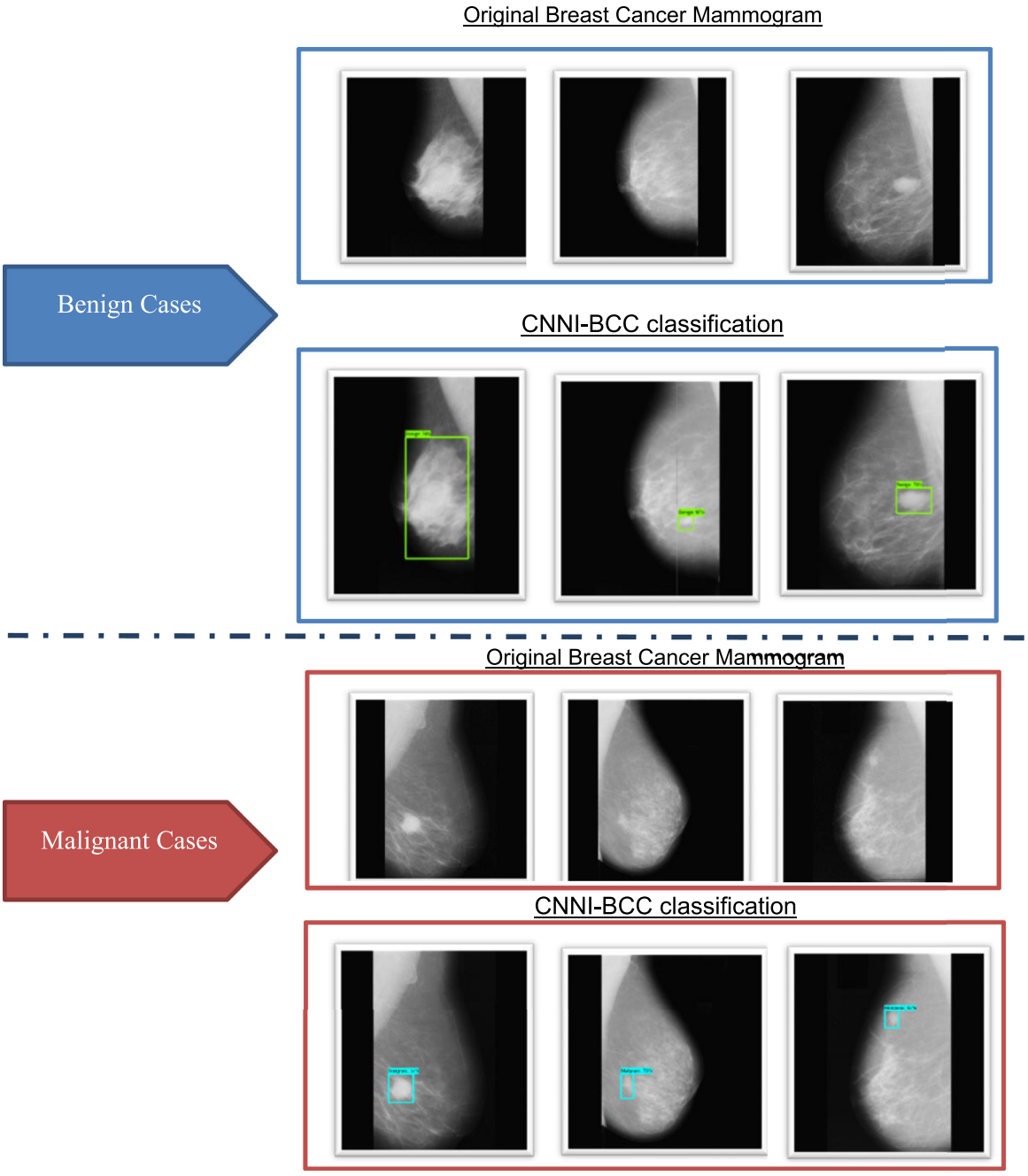

Fig. 20. The CNNI-BCC classification results for several patients.

Table 7
The criterion values and coordinates of the ROC curve for Convolutional Neural Network Improvement for Breast Cancer Classification (CNNI-BCC) against ground truths. [Show].

Criterion	Sensitivity	95% CI	Specificity	95% CI	+LR	95% CI	-LR	95% CI	+PV	95% CI	-PV	95% CI
≥0	100.00	90.7 – 100.0	0.00	0.0 – 2.0	1.00	1.0 – 1.0			17.2	17.2 – 17.2		
>0	89.47	75.2 – 97.1	90.71	85.5 – 94.5	9.63	6.0 – 15.3	0.12	0.05 – 0.3	66.7	55.7 – 76.1	97.6	94.3 – 99.1
>1	0.00	0.0 – 9.3	100.00	98.0 - 100.0			1.00	1.0 – 1.0			82.8	82.8 – 82.8

4.2. CNNI-BCC evaluation on detected breast cancer lesion

Breast cancer lesions are detected and classified through presented work. The detected region are labelled with the matching probability of the breast cancer types. Fig. 20 showed several real patient's breast cancer classification results.

According to the table, the detected region of breast cancer lesion area are labelled as the type of the breast cancer. The computed classification probability are shown on the labelled tag along with the bounding box.

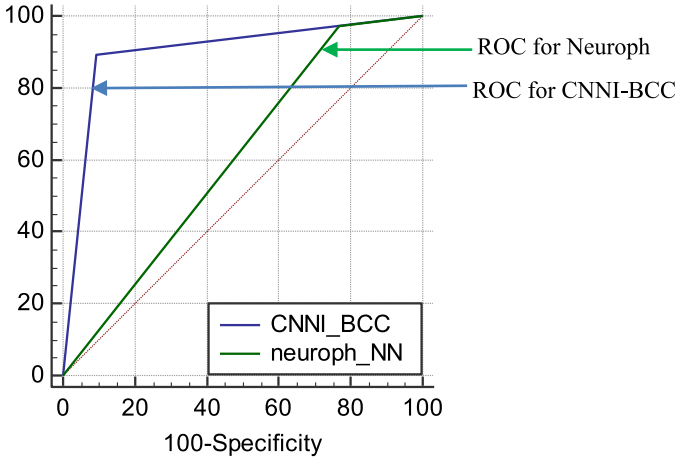

Fig. 21. The ROC curves generated from CNNI-BCC and Neuroph (The Neuroph, 2018).

Table 8
The analysis of ROC curve comparison of CNNI-BCC and Neuroph (The Neuroph, 2018).

Variable	AUC	SE[a]	95% CI[b]
CNNI_BCC	0.901	0.0274	0.854 to 0.937
neuroph_NN	0.602	0.0204	0.534 to 0.667

Table 9
Pairwise comparison of ROC curves.

Difference between areas	0.299
Standard Error[a]	0.0339
95% Confidence Interval	0.233 to 0.366
z statistic	8.838
Significance level	$P < 0.0001$

4.3. ROC curves comparison

The ROC curves generated from CNNI-BCC and Neuroph (The Neuroph, 2018) are compared and discussed. Fig. 21 shows the comparison of the ROC curves from CNNI-BCC and Neuroph (The Neuroph, 2018). The ROC curves are generated based on the 221 patients' classification results. Breast cancer patients are identified as the positive group while normal or healthy patients are indicated as the negative group. Table 8 summarizes the results.

As shown in Table 8, AUC for CNNI-BCC is 0.901 ± 0.0274, which is better than those of Neuroph (The Neuroph, 2018)., i.e., 0.602 ± 0.0204. The pairwise comparison of ROC curves is analysed, and tabulated in Table 9. For pairwise comparison of ROC curves, the calculated significance level P is less than 0.0001. When the calculated p value is smaller than 0.05 ($P < 0.05$), the two ROC curves are significantly different. Hence, the tabulated result shows that CNNI-BCC is better than Neuroph (The Neuroph, 2018).

Based on the 221 real patient subjects, CNNI-BCC has achieved the better performance as compared to Neuroph (The Neuroph, 2018). CNNI-BCC outperforms other relevant methods by having the lowest false positive and false negative rates. The lowest false positive and false negative rates indicate that the chances of false detection of CNNI-BCC are lower than other compared techniques. Therefore, the evaluation outcome ascertained that CNNI-BCC is a better-automated breast cancer lesion classification method.

In Section 4.1, the experimental results between CNNI-BCC and the Mammogram Classification Using Convolutional Neural Networks (MCCNN) (Henry, 2018) are compared. By referring to Fig. 19, CNNI-BCC excels than the MCCNN for the mass argument images and all arguments images by achieving higher accuracy on classification.

In Section 4.2, CNNI-BCC can classify the testing images as malignant, benign and normal classes. The region of suspected cancer lesion mass is labelled with classification result. For the segmentation feature, the presented method can be improved by applying heat map representation of the cancer lesion distribution. This feature can enhance the image quality and provide more information to the medical experts.

In Section 4.3, the conducted experiment and evaluation showed that CNNI-BCC outperforms other methods in terms of having the highest accuracy. The performance can be improved through more real patient datasets. The model can be employed to other mediums such as smartphones to assist medical experts in breast cancer diagnosis.

5. Conclusions

CNNI-BCC method is presented to assist medical doctors in breast cancer diagnosis. Conventionally, medical experts must manually delineate the suspected breast cancer area. Studies suggested that manual segmentation not only takes time, but also relies on the machine and the operator (Ting and Sim 2018, El Atlas, El Aroussi, & Wahbi, 2014). To counter the mentioned issues, CNNI-BCC is designed to implement supervised deep learning neural network for breast cancer classification. The presented work is an attempt to help medical doctors in determining breast cancer lesion. The study was experimented on 221 real patient subjects. The evaluation based on the experimental results showed that CNNI-BCC outperforms existing studies (Saad et al., 2016; Tan et al., 2017) and commercial product, Neuroph (The Neuroph, 2018). CNNI-BCC achieved sensitivity, accuracy, AUC and specificity of 89.47%, 90.50%, 0.901 ± 0.0314 and 90.71%, respectively.

The key contribution of this research is the application of IDBLL with improved CNNBS to detect and classify breast cancer lesion automatically without prior knowledge with respect to its presence. The CNNI-BCC model is superior to the compared methods based on a test set of 221 real patient subjects. The results indicate the potential of CNNI-BCC to analyse the conditions of suspected breast cancer patients during diagnosis.

Conflict of interest

The author(s) declare(s) that there is no conflict of interest regarding the publication of this paper.

Acknowledgements

We would like to thank Mammographic Image Analysis Society (MIAS) (Mammographic Image Analysis Society, 2018) for providing the real patient digital mammogram dataset for research purposes. Fundamental Research Grant Scheme (FRGS) funds this research. FRGS is a national research grant from the Ministry of Education (MOE), Malaysia.

References

Araujo, T., Aresta, G., Castro, E., Rouco, J., Aguiar, P., & Eloy, C. (2017). Classification of breast cancer histology images using convolutional neural networks. *PLoS One, 12*(6), 1–14. doi:10.1371/journal.pone.0177544.

Bogoni, L., Ko, J. P., Alpert, J., Anand, V., Fantauzzi, J., Florin, C. H., et al. (2012). Impact of a computer-aided detection (CAD) system integrated into a picture archiving and communication system (PACS) on reader sensitivity and efficiency for the detection of lung nodules in thoracic CT exams. *Journal of Digital Imaging, 25*(6), 771–781. doi:10.1007/s10278-012-9496-0.

Breast Cancer Statistics. Accessed: 1 February 2018. http://www.breastcancer.org/ .

Breast Cancer Care. Accessed: 5 October 2018. https://www.breastcancercare.org.uk/about-us/media/press-releases/three-quarters-nhs-trusts-health-boards-say-%E2%80%98not-enough%E2%80%99-care .

Chen, Z., & Molloi, S. (2003). Automatic 3D vascular tree construction in CT angiography. *Computerized Medical Imaging and Graphics, 27*(6), 469–479. doi:10.1016/S0895-6111(03)00039-9.

Cheng, J.-Z., Ni, D., Chou, Y.-H., Qin, J., Tiu, C.-M., Chang, Y.-C., et al. (2016). Computer-aided diagnosis with deep learning architecture: applications to breast lesions in US images and pulmonary nodules in CT scans. *Scientific Reports, 6*(1), 24454. doi:10.1038/srep24454.

Chin-Hsing, C., Ann-Shu, L., Jiann-Der, L., & Yang, W. H. (1995). 3D image reconstruction of bladder by nonlinear interpolation. *Mathematical and Computer Modelling, 22*(8), 61–72. doi:10.1016/0895-7177(95)00155-U.

Drew, T., Cunningham, C., & Wolfe, J. (2012). When and why might a Computer Aided Detection (CAD) system interfere with visual search? An eye-tracking study. *Academic Radiology, 19*(10), 1260–1267. doi:10.1016/j.acra.2012.05.013.

El Atlas, N., El Aroussi, M., & Wahbi, M. (2014). Computer-aided breast cancer detection using mammograms: A review. In *Proceedings of the 2nd world conference on complex systems, WCCS* (pp. 626–631). doi:10.1109/ICoCS.2014.7060995.

El-Zahraa, F., El-Gamal, A., Mohammed, E., & Ahmed, A. (2016). Current trends in medical image registration and fusion. *Egyptian Informatics Journal, 17*(1), 99–124. doi:10.1016/j.eij.2015.09.002.

Goodfellow, I., Bengio, Y., & Courville, A. (2016). *Deep Learning*. Cambridge: The MIT Press.

Hellquist, B. N., Czene, K., Hjälm, A., Nyström, L., & Jonsson, H. (2015). Effectiveness of population-based service screening with mammography for women ages 40 to 49 years with a high or low risk of breast cancer: Socioeconomic status, parity, and age at birth of first child. *Cancer, 121*(2), 251–258. doi:10.1002/cncr.29011.

Henry, Z.Mammogram Classification Using Convolutional Neural Networks. Accessed: 02 October 2017. http://ehnree.github.io/documents/papers/mammogram_conv_net.pdf .

Hua, K.-L., Hsu, C.-H., Hidayati, S. C., Cheng, W.-H., & Chen, Y.-J. (2015). Computer-aided classification of lung nodules on computed tomography images via deep learning technique. *OncoTargets and Therapy, 8*, 2015–2022. doi:10.2147/OTT.S80733.

Hubel, D. H., & Wiesel, T. N. (1968). Receptive fields and functional architecture of monkey striate cortex. *The Journal of Physiology, 195*(1), 215–243. doi:10.1113/jphysiol.1968.sp008455.

Kallenberg, M., Petersen, K., Nielsen, M., Ng, A. Y., Diao, P., Igel, C., et al. (2016). Unsupervised deep learning applied to breast density segmentation and mammographic risk scoring. *IEEE Transactions on Medical Imaging, 35*(5), 1322–1331. doi:10.1109/TMI.2016.2532122.

Karpathy, A. (2018). *CS231n: Convolutional neural networks for visual recognition*. Stanford University http://cs231n.stanford.edu/ Accessed: 2 October 2017.

Krizhevsky, A., Sutskever, I., & Hinton, G. E. (2012). ImageNet classification with deep convolutional neural networks. In *Proceedings of the Advances in Neural Information Processing Systems* (pp. 1097–1105).

Kumar, D., Wong, A., & Clausi, D. A. (2015). Lung nodule classification using deep features in CT Images. In Proceedings of the *12th conference on computer and robot vision* (pp. 133–138). doi:10.1109/CRV.2015.25.

Le, A. H. T., Liu, B., & Huang, H. K. (2009). Integration of computer-aided diagnosis/detection (CAD) results in a PACS environment using CAD-PACS toolkit and DICOM SR. *International Journal of Computer Assisted Radiology and Surgery, 4*(4), 317–329. doi:10.1007/s11548-009-0297-y.

Lee, J.-G., Jun, S., Cho, Y.-W., Lee, H., Kim, G. B., & Seo, J. B. (2017). Deep learning in medical imaging: general overview. *Korean Journal of Radiology, 18*(4), 570. doi:10.3348/kjr.2017.18.4.570.

Lewis, T. C., Pizzitola, V. J., Giurescu, M. E., Eversman, W. G., Lorans, R., & Robinson, K. A. ,&Patel,B. K. (2017). Contrast-enhanced digital mammography: A single-institution experience of the first 208 cases. *Breast Journal, 23*(1), 67–76. doi:10.1111/tbj.12681.

Liu, S., Liu, S., Cai, W., Pujol, S., Kikinis, R., & Feng, D. (2014). Early diagnosis of Alzheimer's disease with deep learning. In *Proceedings of the IEEE 11th international symposium on biomedical imaging (ISBI)* (pp. 1015–1018). doi:10.1109/ISBI.2014.6868045.

Liu, W., Anguelov, D., Erhan, D., Szegedy, C., Reed, S., & Fu, C. Y. ,&Berg,A. C. (2016). SSD: Single shot multibox detector. *Computer Vision and Pattern Recognition*. https://arxiv.org/abs/1512.02325.

Mammographic Image Analysis Society (MIAS). Accessed: 25 January 2018. http://www.mammoimage.org/databases/ .

Mohebian, M. R., Marateb, H. R., Mansourian, M., Mañanas, M. A., & Mokarian, F. (2017). A Hybrid Computer-aided-diagnosis System for Prediction of Breast Cancer Recurrence (HPBCR) Using Optimized Ensemble Learning. *Computational and Structural Biotechnology Journal, 15*, 75–85. doi:10.1016/j.csbj.2016.11.004.

MIMS News. Accessed: 4 October 2018. https://today.mims.com/malaysia-needs-more-oncologists-and-specialists-to-treat-cancer-patients .

Neuroph. Accessed: 25 January 2018. http://neuroph.sourceforge.net/ .

Onega, T., Goldman, L. E., Walker, R. L., Miglioretti, D. L., Buist, D. S., Taplin, S., et al. (2016). Facility mammography volume in relation to breast cancer screening outcomes. *Journal of Medical Screening, 23*(1), 31–37. doi:10.1177/0969141315595254.

Ozmen, N., Dapp, R., Zapf, M., Gemmeke, H., Ruiter, N. V., & Van Dongen, K. W. A. (2015). Comparing different ultrasound imaging methods for breast cancer detection. *IEEE Transactions on Ultrasonics, Ferroelectrics, and Frequency Control, 62*(4), 637–646. doi:10.1109/TUFFC.2014.006707.

Qin, C., Tao, D., Shi, Y. H., & Song, Z. J. (2018). Computer-aided detection in chest radiography based on artificial intelligence: A survey. *BioMedical Engineering OnLine, 17*(113). doi:10.1186/s12938-018-0544-y.

Roganovic, D., Djilas, D., Vujnovic, S., Pavic, D., & Stojanov, D. (2015). Breast MRI, digital mammography and breast tomosynthesis: Comparison of three methods for early detection of breast cancer. *Bosnian Journal of Basic Medical Sciences, 15*(4), 64–68. doi:10.17305/bjbms.2015.616.

Saad, G., Khadour, A., & Kanafani, Q. (2016). ANN and Adaboost application for automatic detection of microcalcifications in breast cancer. *Egyptian Journal of Radiology and Nuclear Medicine, 47*(4), 1803–1814. doi:10.1016/j.ejrnm.2016.08.020.

Suk, H., & Shen, D. (2013). Deep learning-based feature representation for AD/MCI classification. In *Lecture notes in computer science (including subseries Lecture notes in artificial intelligence and lecture notes in bioinformatics): 8150* (pp. 583–590). LNCS. doi:10.1007/978-3-642-40763-5_72.

Suk, H., Lee, S. W., & Shen, D. (2014). Hierarchical feature representation and multimodal fusion with deep learning for AD/MCI diagnosis. *NeuroImage, 101*, 569–582. doi:10.1016/j.neuroimage.2014.06.077.

Tan, Y. J., Sim, K. S., & Ting, F. F. (2017). Breast cancer detection using convolutional neural networks for mammogram imaging system. In *Proceedings of the international conference on robotics, automation and sciences (ICORAS)* (pp. 1–5). doi:10.1109/ICORAS.2017.8308076.

Tang, A., Tam, R., Cadrin-Chenevert, A., Guest, W., Chong, J., Barfett, J., Geis, R., et al. (2018). Canadian association of radiologists white paper on artificial intelligence in radiology. *Canadian Association of Radiologists Journal, 69*(2), 120–135. doi:10.1016/j.carj.2018.02.002.

Ting, F. F., & Sim, K. S. (2018). Self-regulated multilayer perceptron neural network for breast cancer classification. In *Proceedings of the international conference on robotics, automation and sciences (ICORAS)* (In-press).

Wang, D., Khosla, A., Gargeya, R., Irshad, H., & Beck, A. H. (2016). *Deep learning for identifying metastatic breast cancer*, 1–6. arXiv Preprint https://people.csail.mit.edu/khosla/papers/arxiv2016_Wang.pdf.

Wang, L. (2017). Early diagnosis of breast cancer. *Sensors, 17*(7), 1572. doi:10.3390/s17071572.

Wang, S., & Summers, R. M. (2012). Machine Learning and Radiology. *Medical Image Analysis, 16*(5), 933–951. doi:10.1016/j.media.2012.02.005.

Welter, P., Hocken, C., Deserno, T. M., Grouls, C., & Günther, R. W. (2010). Workflow management of content-based image retrieval for CAD support in PACS environments based on IHE. *International Journal of Computer Assisted Radiology and Surgery, 5*(4), 393–400. doi:10.1007/s11548-010-0416-9.

Xavier, C., Blykers, A., Vaneycken, I., D'Huyvetter, M., Heemskerk, J., Lahoutte, T., et al. (2016). 18F-nanobody for PET imaging of HER2 overexpressing tumors. *Nuclear Medicine and Biology, 43*(4), 247–252. doi:10.1016/j.nucmedbio.2016.01.002.

Youlden, D. R., Cramb, S. M., Dunn, N. A. M., Muller, J. M., Pyke, C. M., & Baade, P. D. (2012). The descriptive epidemiology of female breast cancer: an international comparison of screening, incidence, survival and mortality. *Cancer Epidemiology, 36*(3), 237–248. doi:10.1016/j.canep.2012.02.007.

Zhou, Z. (2007). Data security assurance in CAD-PACS integration. *Computerized Medical Imaging and Graphics, 31*(4–5), 353–360. doi:10.1016/j.compmedimag.2007.02.013.